Combined Analysis: Texture, Structure, Residual Stress, Microstructure … characterization using rays scattering

D. Chateigner

CRISMAT-CNRS-ENSICAEN

Université de Caen Normandie,Normandie Université

LOMC, Université Le Havre Normandie, 8th Feb. 2024

Retrospective

- Rietveld: *Acta Cryst. (1967), J. Appl. Cryst (1969)*: NPD
- Rietveld on combined powder measurements: GSAS by Larson & Von Dreele, Fullprof by Rodriguez-Carvajal, Jana by Petricek …

- Rietveld + QTA (WIMV): Lutterotti, Matthies, Wenk *J. Appl. Phys. (1997)*

- ESQUI EU FP6 project (1999-2003):

-- Rietveld (+ layers + QMA + RSA + E-WIMV): Morales *et al. Mat. Sci. For.* (2002), Lutterotti et al. *Thin Sol. Films* (2004)

-- + XRR + prop. Tensor homogeneization: Extended Rietveld,
Combined Analysis *Wiley-ISTE (2010), Int. Tab. Vol H (2019)*

- Electron Diffraction Pattern (2-waves Blackman dyn. Corr.): Boullay *et al. Acta Cryst A (2014)*
- X-ray Fluorescence (incl. Grazing incidence): Caby *et al. Spect. Acta B (2015)*
- SOLSA EU 2020 Raw Materials project (2016-2021):

+ Raman spec.: El Mendili *et al. ACS Earth & Space Chem. (2019)* + ROD *J. Appl. Cryst. (2019)*

Scattering "sees"

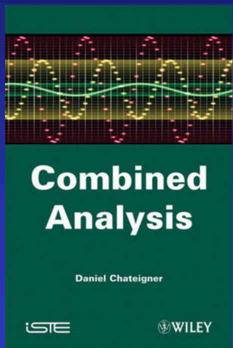

XRD

Texture
$f(g)_{\Phi,L}$

Structure
$|F_{\mathbf{h}}|^2_{\Phi,L}$

Real samples
Layered samples
thicknesses
roughnesses
$\rho(z)$…

Residual Stress
$<C_{ijkl}(g)>_{\Phi,L}$

defects (0D .. nD)
broadening
asymmetry

Raman, IR

Phase ID

Phase
$S_{\Phi,L}$

Element ID

XRF

Structure-Texture bias using individual analyses

B. Maestracci, PhD

	1 θ-2θ diagram	864 (χ□φ) 2θ diagrams
	Atomic positions (Å)	*Atomic positions (Å)*
Single crystal	-	z_{Al}: 0.35222(4) x_O: 0.3063(2)
March-Dollase 00ℓ (100%)	z_{Al}: 0.35219(2) x_O: 0.3054(2)	-
March-Dollase 00ℓ (99%) ℎ00 (1%)	z_{Al}: 0.35232(2) x_O: 0.3094(2)	-
ODF E-WIMV 3.75°	-	**z_{Al}: 0.352225(7)** **x_O: 0.30633(5)**

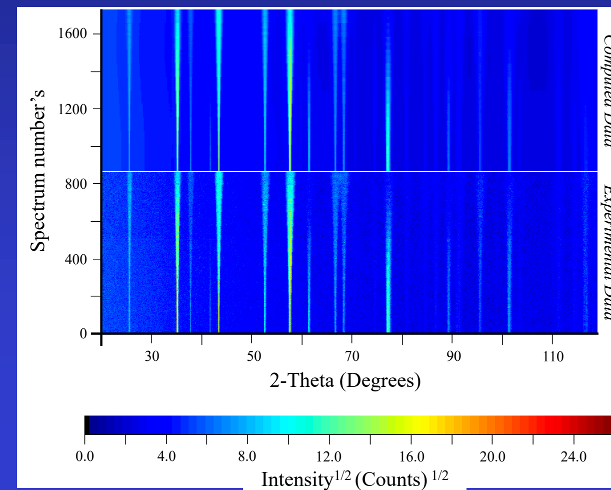

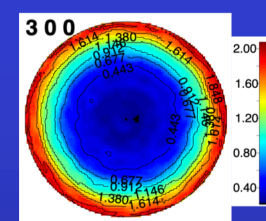

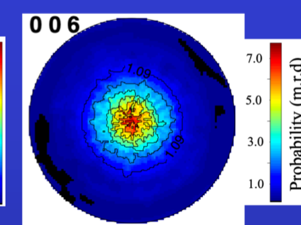

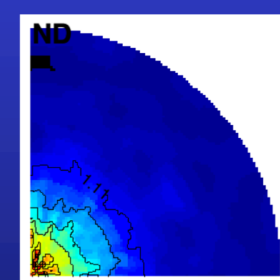

Extended Rietveld

$$y_c(\mathbf{y_S},\theta,\eta) = y_b(\mathbf{y_S},\theta,\eta) + I_0 \sum_{i=1}^{N_L} \sum_{\Phi=1}^{N_\Phi} \frac{\nu_{i\Phi}}{V_{c\Phi}^2} \sum_h Lp(\theta) j_{\Phi h} \left|F_{\Phi h}\right|^2 \Omega_{\Phi h}(\mathbf{y_S},\theta,\eta) P_{\Phi h}(\mathbf{y_S},\theta,\eta) A_{i\Phi}(\mathbf{y_S},\theta,\eta)$$

Phase %

Structure

Texture

Microstructure
Strain-Stress

Layering

XRF: Shermann, De Boer

$$dI_{\zeta jk} \propto \overbrace{e^{-\mu_{s,E_0} \frac{z}{\sin \phi_i}}}^{1.} \overbrace{W_\zeta \left(\frac{\tau_j}{\rho}\right)_{\zeta E_0} \rho_s dz}^{2.} \cdot$$

$$\cdot \underbrace{\omega_{\zeta j}}_{3.} \underbrace{p_{\zeta jk}}_{4.} \underbrace{e^{-\mu_{s,E_{\zeta jk}} \frac{z}{\sin \phi_f}}}_{5.} \underbrace{\epsilon_{E_{\zeta jk}}}_{6.}$$

1. attenuation to depth z
2. photoelectric absorption in layer dz
3. fluorescence yield
4. transition probability
(relative intensity of lines in shell)
5. attenuation to the detector
6. detector efficiency

Texture:

$$P_h(\mathbf{y}_S) = \int_{\tilde{\varphi}} f(g,\tilde{\varphi})\,d\tilde{\varphi}$$

E-WIMV, components, Harmonics, Exp. Harmonics …

Strain-Stress:

$$\langle S\rangle_{geo}^{-1} = \left[\prod_{m=1}^{N} S_m^{\nu_m}\right]^{-1} = \prod_{m=1}^{N} S_m^{-\nu_m} = \prod_{m=1}^{N} \left(S_m^{-1}\right)^{\nu_m} = \left\langle S^{-1}\right\rangle_{geo} = \langle C\rangle_{geo}$$

Geometric mean, Voigt, Reuss, Hill …

Layering:

$$A_{i\Phi} = \frac{\nu_{i\Phi}\sin\theta_i\sin\theta_o}{\bar{\mu}_i(\sin\theta_i+\sin\theta_o)}\left\{1-e^{-\bar{\mu}_i\tau_i W}\right\}\prod_{k<i} e^{-\bar{\mu}_k\tau_k W}$$

$$W = \frac{1}{\sin\theta_i}+\frac{1}{\sin\theta_o}$$

Stacks, coatings, multilayers …

Line Broadening:

Crystallite sizes, shapes, μstrains, distributions

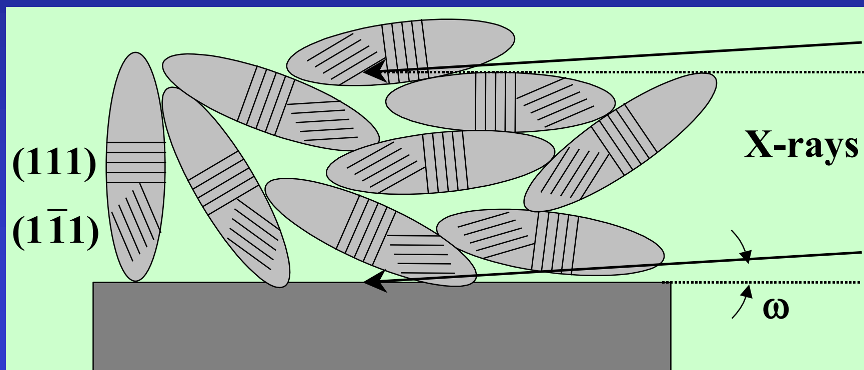

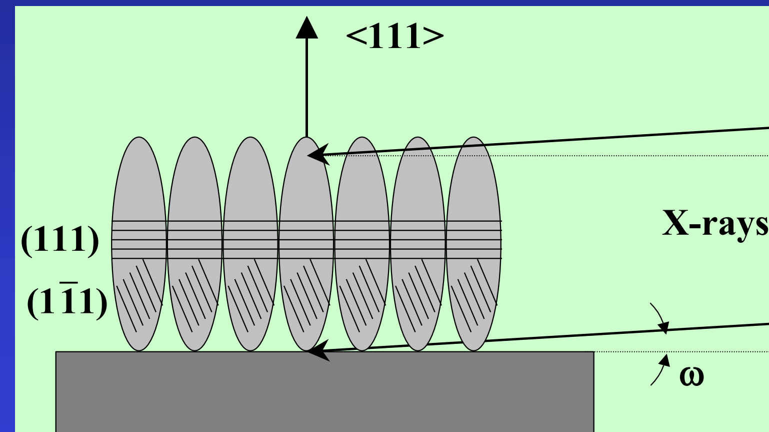

- Texture helps the "real" mean shape determination

$$\langle R_{\vec{h}} \rangle = \sum_{\ell=0}^{L} \sum_{m=0}^{\ell} R_\ell^m K_\ell^m(\chi,\varphi)$$

Symmetrised spherical harmonics

$$K_\ell^m(\chi,\varphi) = P_\ell^m(\cos\chi)\cos(m\varphi) + P_\ell^m(\cos\chi)\sin(m\varphi)$$

$$\langle R_{\mathbf{h}} \rangle = R_0 + R_1 P_2^0(x) + R_2 P_2^1(x)\cos\varphi + R_3 P_2^1(x)\sin\varphi + R_4 P_2^2(x)\cos 2\varphi + R_5 P_2^2(x)\sin 2\varphi + \ldots$$

$$\langle \varepsilon_{\mathbf{h}}^2 \rangle E_{\mathbf{h}}^4 = E_1 h^4 + E_2 k^4 + E_3 \ell^4 + 2E_4 h^2 k^2 + 2E_5 \ell^2 k^2 + 2E_6 h^2 \ell^2 + 4E_7 h^3 k + 4E_8 h^3 \ell + 4E_9 k^3 h + 4E_{10} k^3 \ell + 4E_{11} \ell^3 h + 4E_{12} \ell^3 k + 4E_{13} h^2 k \ell + 4E_{14} k^2 h \ell + 4E_{15} \ell^2 k h$$

Specular reflectivity: **q**=(0,0,z)

- Fresnel:

$$R(\mathbf{q}) = \left| \frac{q_z - \sqrt{q_z^2 - q_c^2 + \frac{32 i\pi^2 \beta}{\lambda^2}}}{q_z + \sqrt{q_z^2 - q_c^2 + \frac{32 i\pi^2 \beta}{\lambda^2}}} \right|^2 \delta q_x \delta q$$

- matrix:

$$R^{flat} = \frac{r_{0,1}^2 + r_{1,2}^2 + 2 r_{0,1} r_{1,2} \cos 2k_{Z,1} h}{1 + r_{0,1}^2 r_{1,2}^2 + 2 r_{0,1} r_{1,2} \cos 2k_{Z,1} h}$$

- Born approximation:
  Electron Density Profile

$$R(q_z) = r.r^* = R_F(q_z) \left| \frac{1}{\rho_s} \int_{-\infty}^{+\infty} \frac{d\rho(z)}{dz} e^{i q_z z} dz \right|^2$$

- Roughness:

$$R^{rough}(q_z) = R(q_z) \exp(-q_{z,0} q_{z,1} \sigma^2) \quad \text{Low-angles (reflectivity)}$$

$$S_R = 1 - p \exp(-q) + \text{p} \exp\left(\frac{\text{-q}}{\sin\theta} \right) \quad \text{high-angle (Suortti)}$$

$\bar{1}$

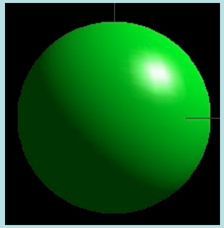

R_0

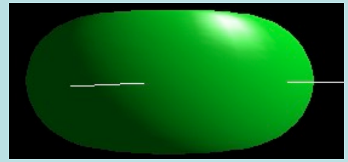

R_0, $R_1 < 0$

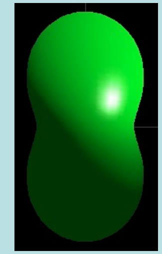

R_0, $R_1 > 0$

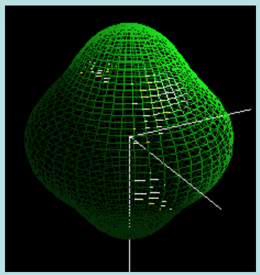

R_0, $R_6 > 0$

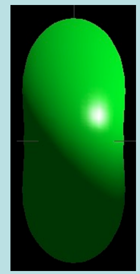

R_0,
R_2 and $R_6 > 0$

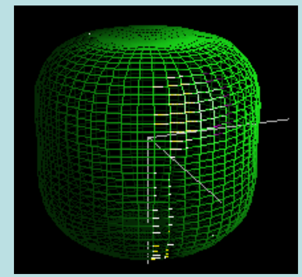

R_0, $R_6 < 0$

6/m

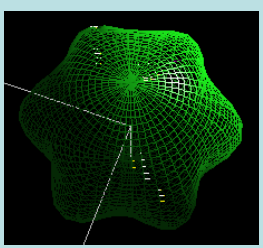

R_0, $R_4 > 0$

m3m

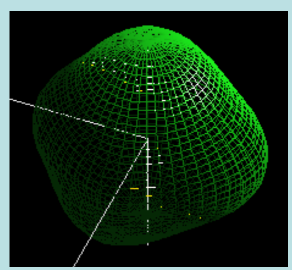

R_0, $R_1 > 0$

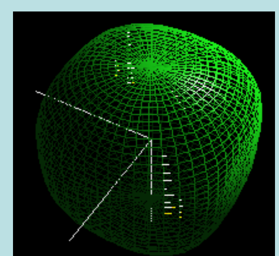

R_0, $R_1 < 0$

Combined Analysis approach

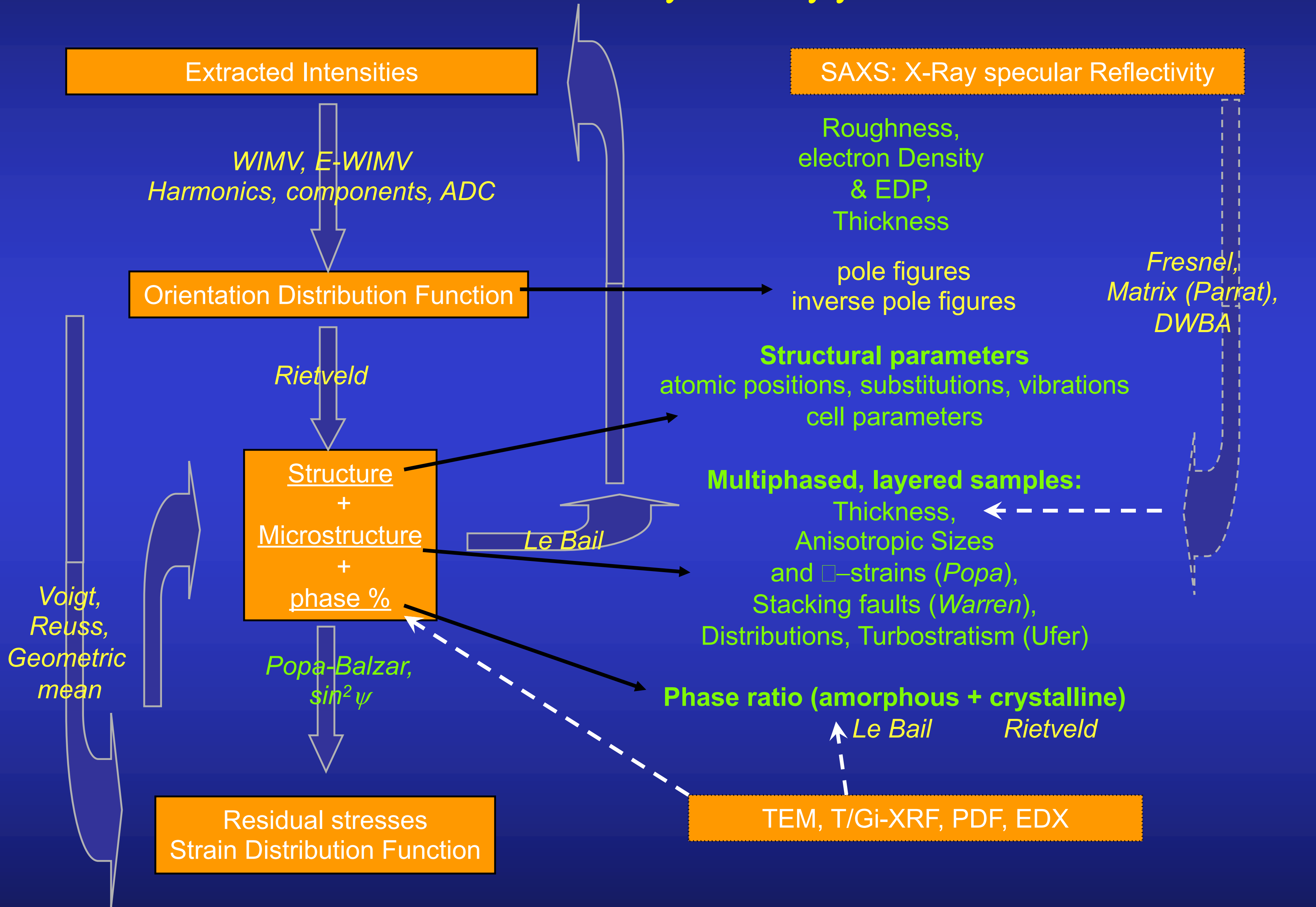

XRD-XRF-Raman-IR Combined Analysis

$$I_{aj} = \frac{\lambda}{hc} C_{aj} \frac{\tau_{aj}}{\mu_{j\lambda}/\rho_j} J_{aj} \omega_a g_a exp\left\{ -\sum_{n=1}^{j-1} \frac{\mu_{na} d_n}{sin\Psi_d} \right\} S_1 \int_0^{d_j} dz \left(\frac{-\partial P_{jz}}{\partial z} \right) exp\left(\frac{\mu_{ja} z}{sin\Psi_d} \right)$$

IR

XRF-GiXRF- TXRF
EDS

Databases
COD-ROD-MPOD

Raman

$$I_{(e_s,e_0)} = I_0 \frac{\hbar}{2\omega_m} (n_m + 1) \frac{(\omega_0 - \omega_m)^4}{c^4} \left| e_s . \alpha_{ij}^m . e_0 \right|^2$$

XRR

$$r = \frac{M_{12}}{M_{22}} = \frac{r_{01} + r_{12} e^{-2iq_{1z}h}}{1 + r_{01} r_{12} e^{-2iq_{1z}h}}$$

Diffraction extended Rietveld (n, X, e^-)

$$y_c(\mathbf{y_S}, \theta, \eta) = y_b(\mathbf{y_S}, \theta, \eta) + I_0 \sum_{i=1}^{N_L} \sum_{\Phi=1}^{N_\Phi} \frac{\nu_{i\Phi}}{V_{c\Phi}^2} \sum_h Lp(\theta) j_{\Phi h} \left| F_{\Phi h} \right|^2 \Omega_{\Phi h}(\mathbf{y_S}, \theta, \eta) P_{\Phi h}(\mathbf{y_S}, \theta, \eta) A_{i\Phi}(\mathbf{y_S}, \theta, \eta)$$

COD ⇐⇒ ROD

www.crystallography.net

solsa.crystallography.net/rod/

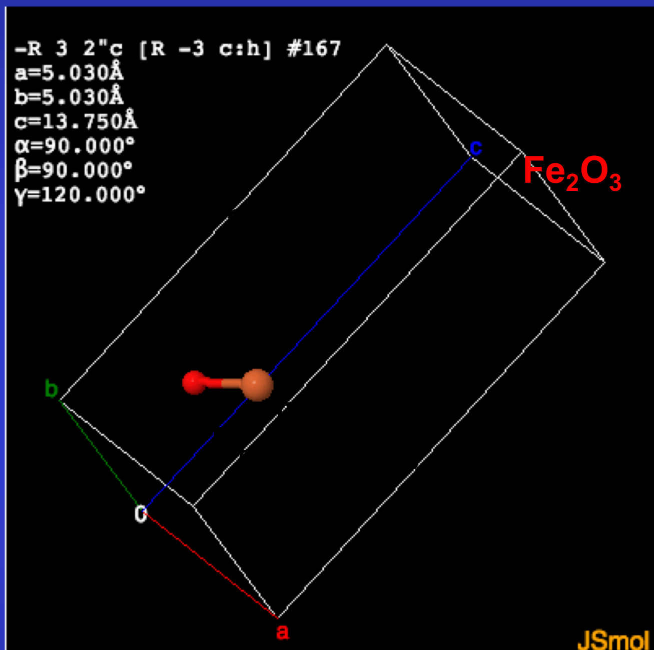

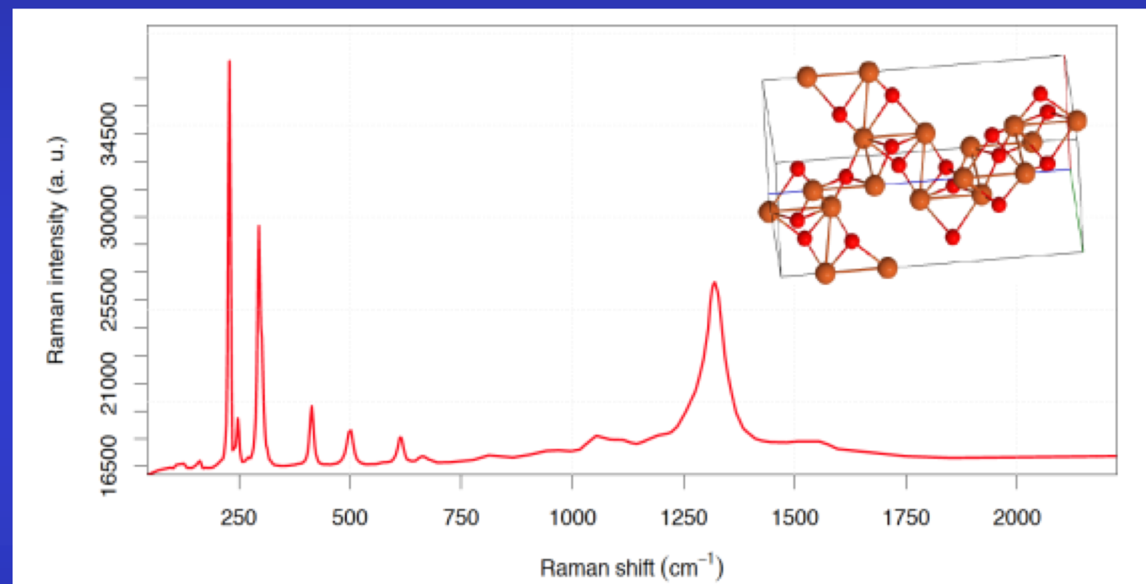

COD ID 1546383 ⇐⇒ ROD ID 1000002

Grazulis et al. *J. Appl. Cryst.* **42** (2009) 726

El Mendili et al. *J. Appl. Cryst.* **52** (2019) 618

XRR, EDP (dynamic correction), Raman

…

Combined Analysis cost function

$$WSS = \sum_{t=1}^{N_p} u_t \sum_{i=0}^{N_t} w_{it} \left(y_{itc} - y_{ito} \right)^2$$

w_{it} : weight for each pattern (usually $1/y_i = \sigma^2$)
u_t : weight for each pattern set t (XRD, XRF …)

EMT nanocrystalline zeolite

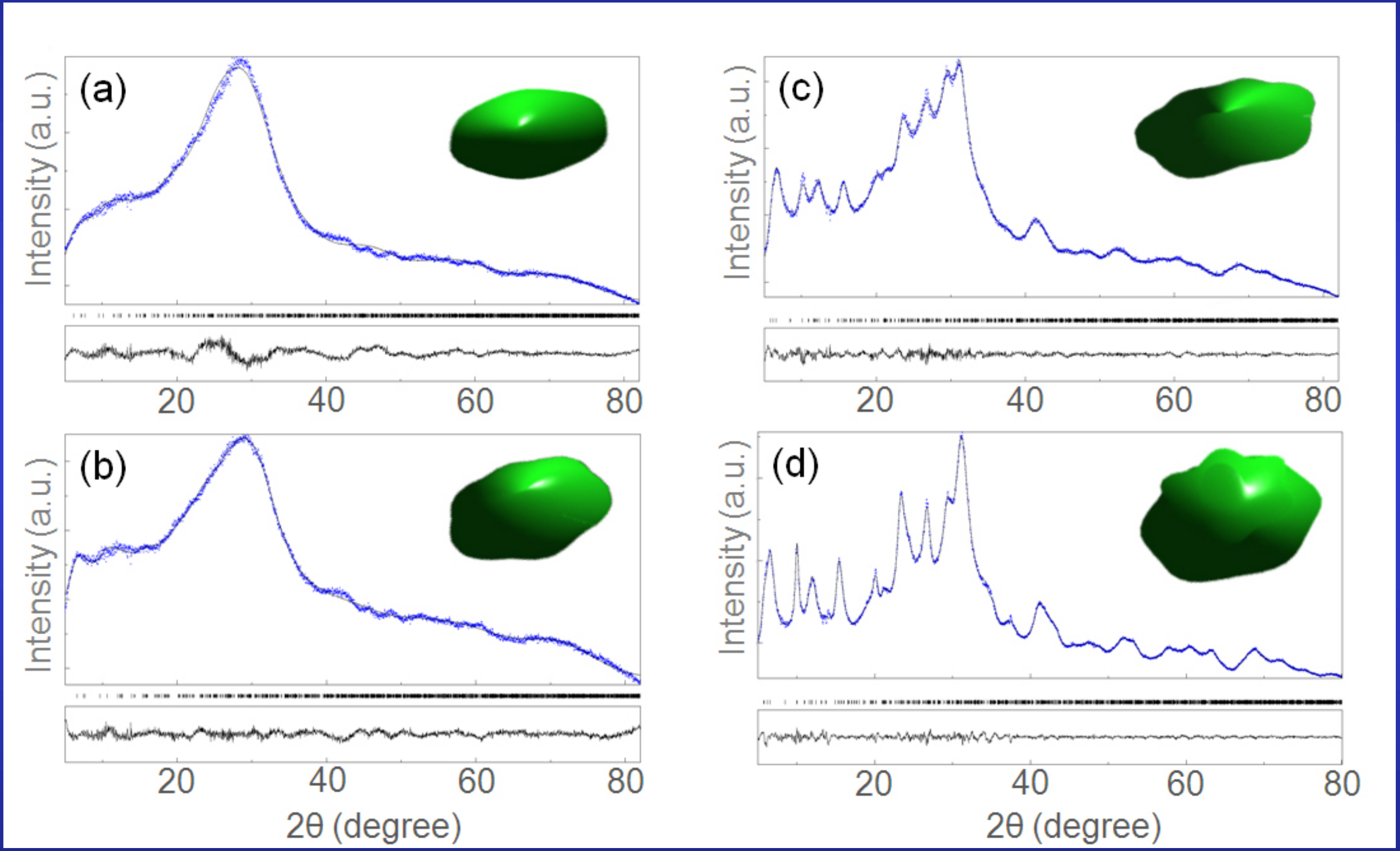

Ng et al. *Science* **335** (2012) 70

Carbon microfibre

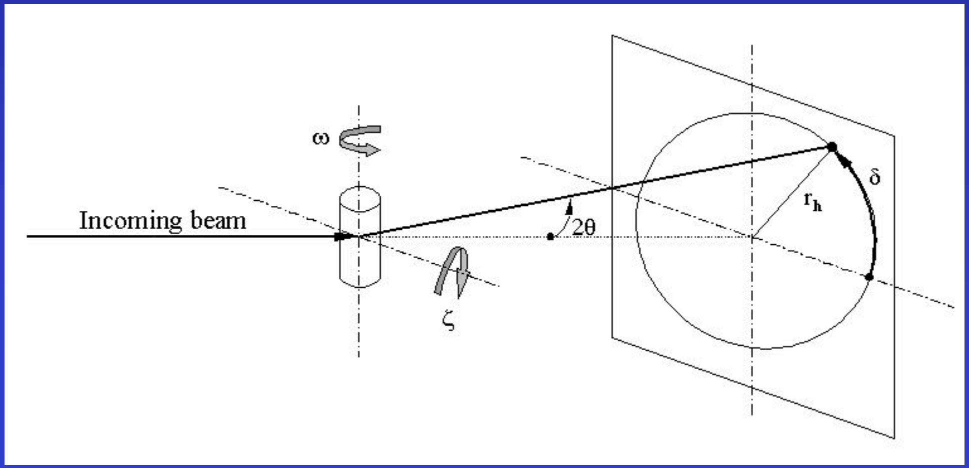

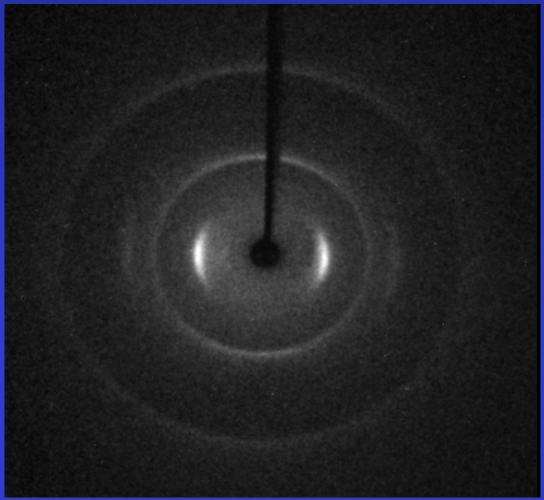

1 fibre (7 microns diameter): CCD Kappa diffractometer

Planar texture Component
Ufer turbostractic model

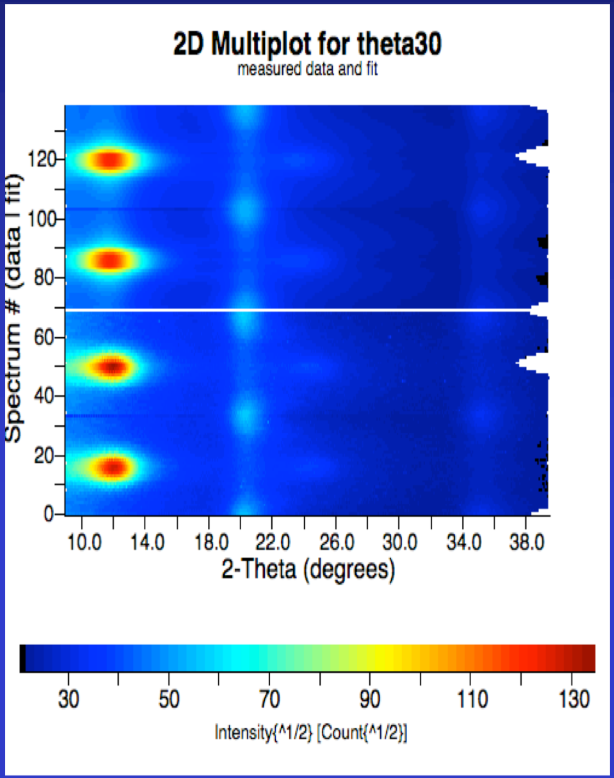

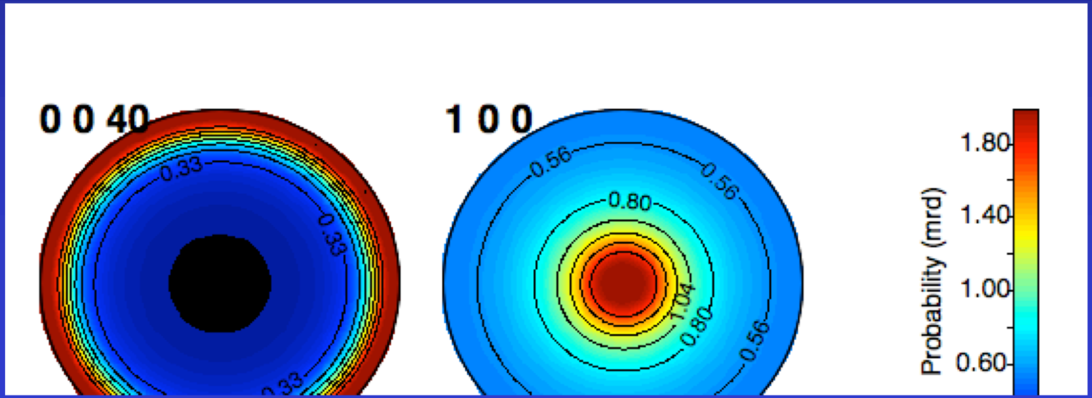

	A(nm)	C(nm)	Orientation FWHM(°)	Max 00l pole figure (m.r.d.)	Crystallite size along c (nm)	Crystallite size along a (nm)	Global microstrain (rms)
C1B1	0.23589(7)	0.6821(1)	21.6(1)	1.95	2.1(4)	2.2(4)	0.0152(10)
C2B1	0.23746(5)	0.68915(8)	18.75(6)	2.05	2.3(2)	2.5(2)	0.0154(11)
C3B1	0.23734(5)	0.69233(9)	18.63(6)	2.04	2.4(3)	2.7(5)	0.0136(6)
C3B2	0.23716(4)	0.69389(9)	19.87(7)	1.98	2.4(4)	2.5(4)	0.0150(4)
C3B3	0.23656(4)	0.68980(8)	19.16(6)	1.99	2.5(6)	2.3(5)	0.0168(8)

Turbostratic phyllosilicate aggregates

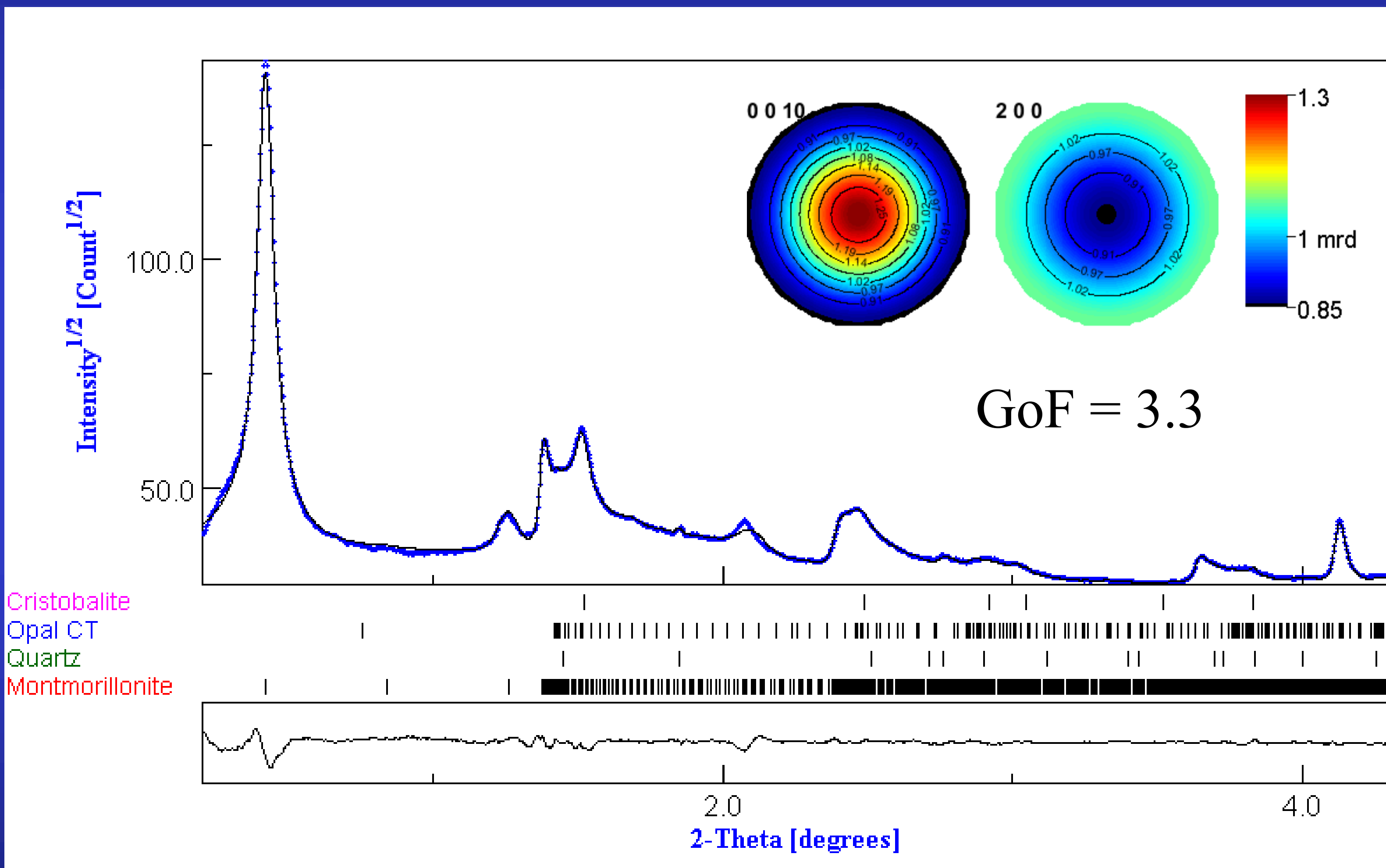

V%
1.45(2)
6.6(1)
0.19(1)
91.8(3)

Minimum experimental requirements

1D or 2D Detector +
4-circle diffractometer
(CRISMAT – ANR EcoCorail)

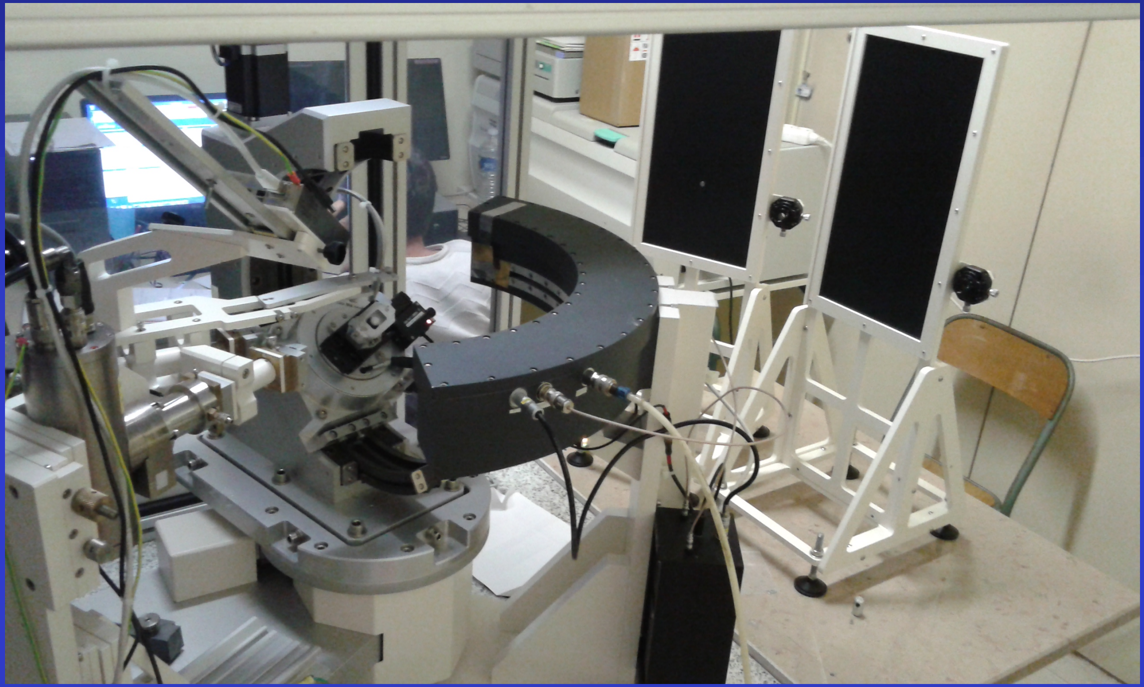

~1000 experiments (2θ diagrams)
in as many sample orientations

+

Instrument calibration
(peaks widths and shapes,
misalignments, defocusing …)

$Mg_{0.75}Fe_{0.25}O$ high pressure experiments

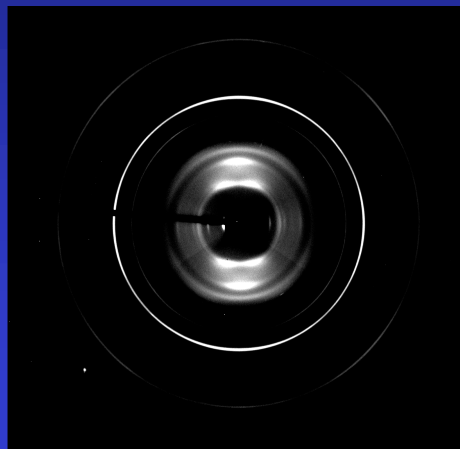

E-WIMV + geo

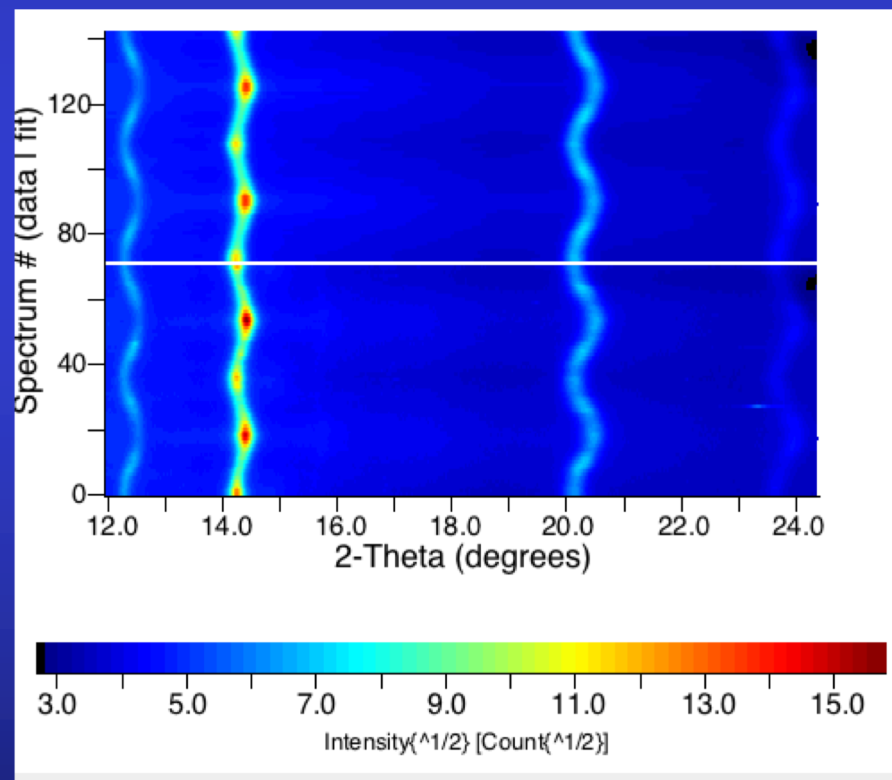

a = 3.98639(3) Å

<t> = 46.8(3) Å

<ε> = 0.00535(1)

σ_{33} = -861(3) MPa

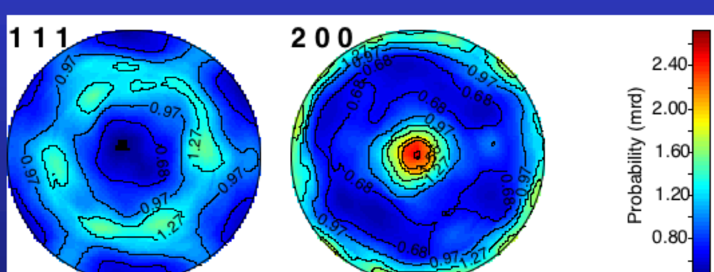

EDP: Microstructure of nanocrystalline materials: TiO2 rutile

- *quantitative analysis of electron diffraction ring pattern ?*

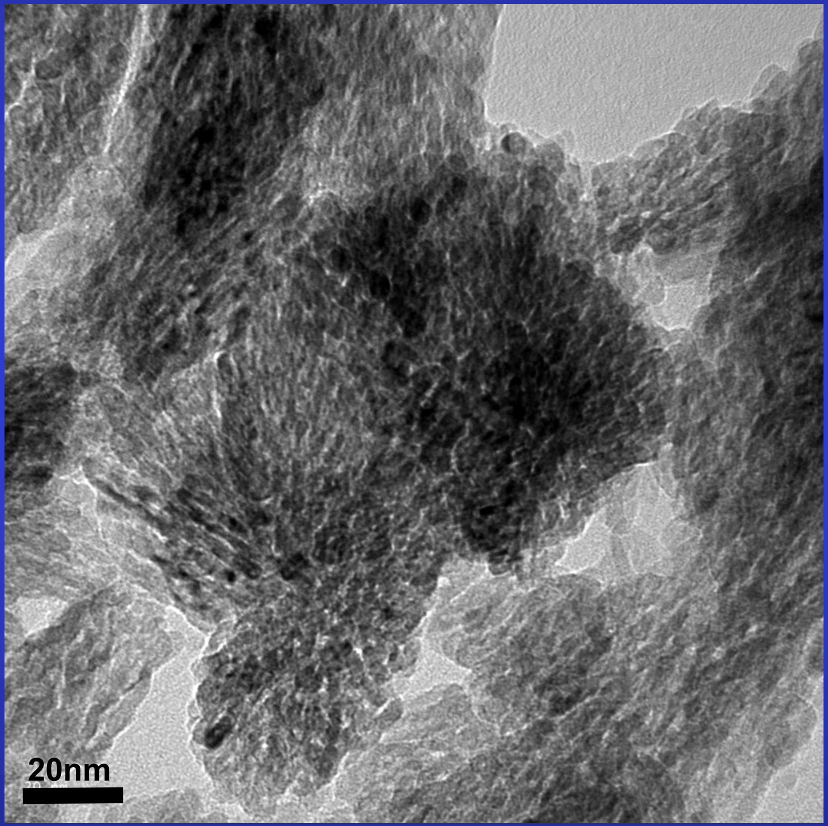

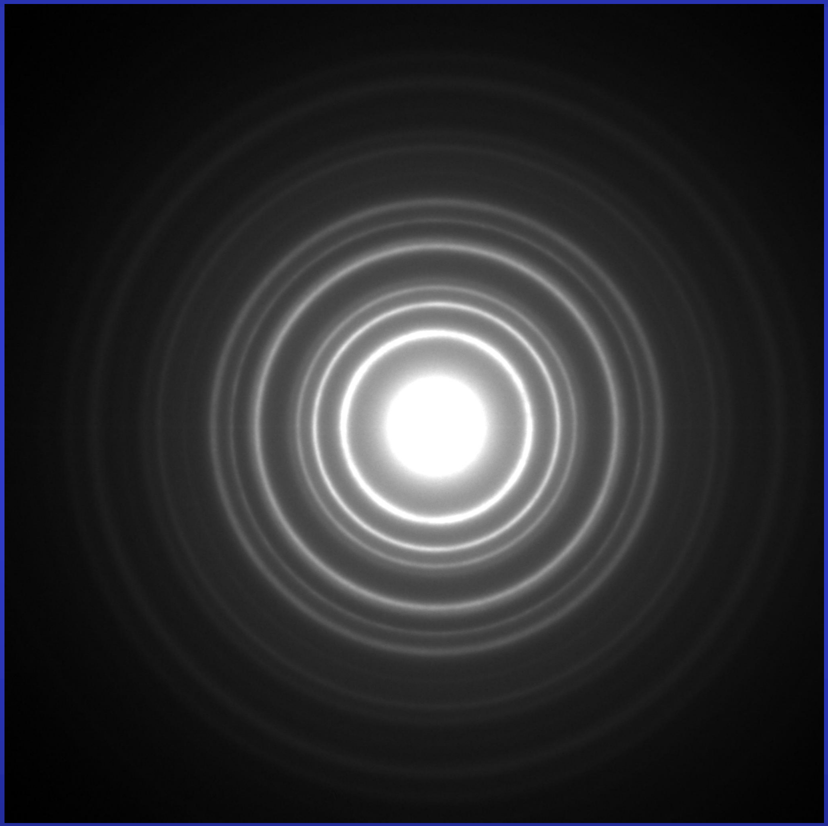

FEI Tecnai G2 (300kV) with an Ultrascan 1000 (2048x2048 14μm pixels)

Paterns taken from +25° to -25° (step 5°) tilts: thin film prepared for TEM plan view

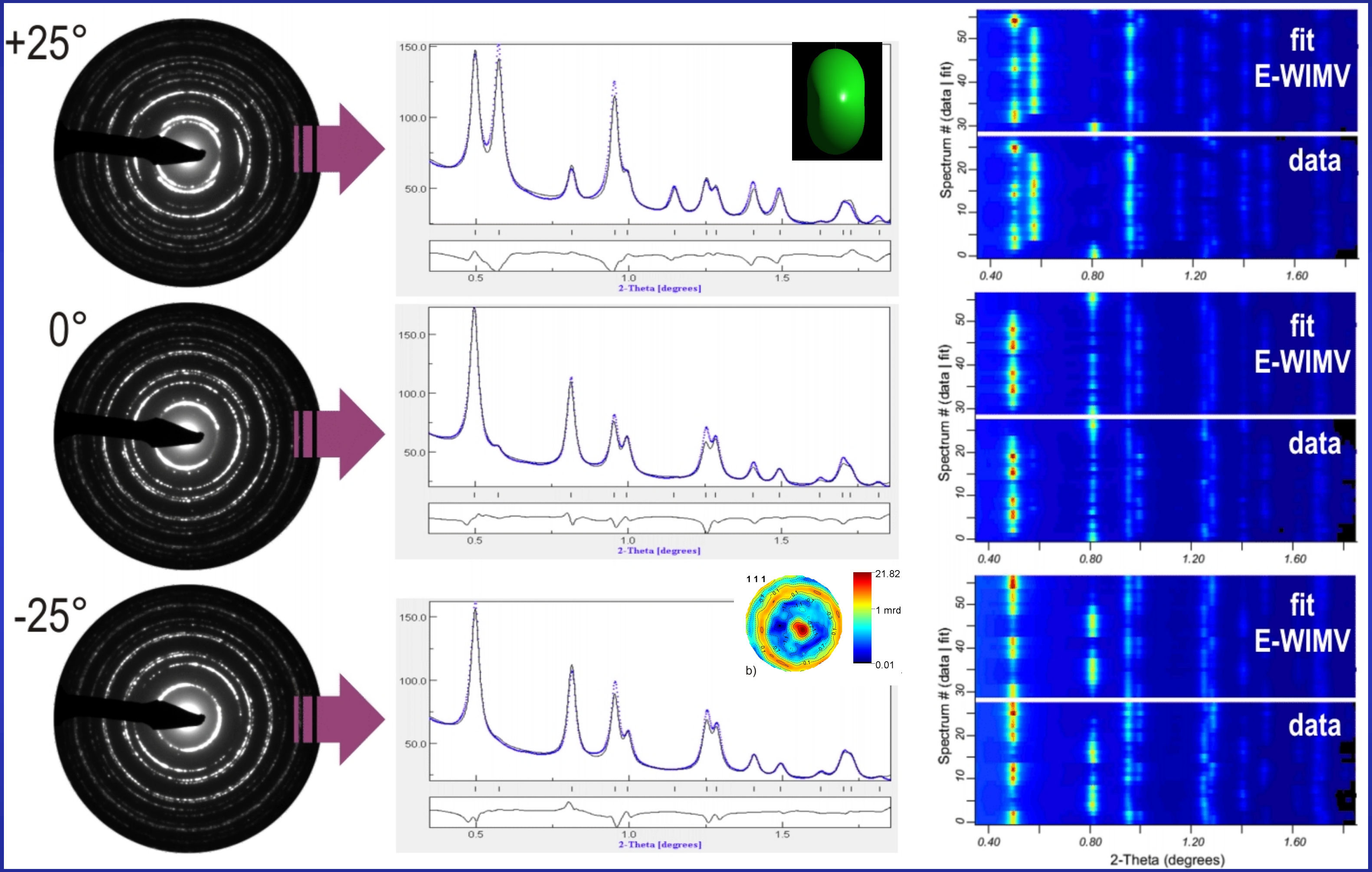

Boullay et al. *Acta Cryst. A* **70** (2014) 448

Combined XRR, XRD & GiXRF Analysis

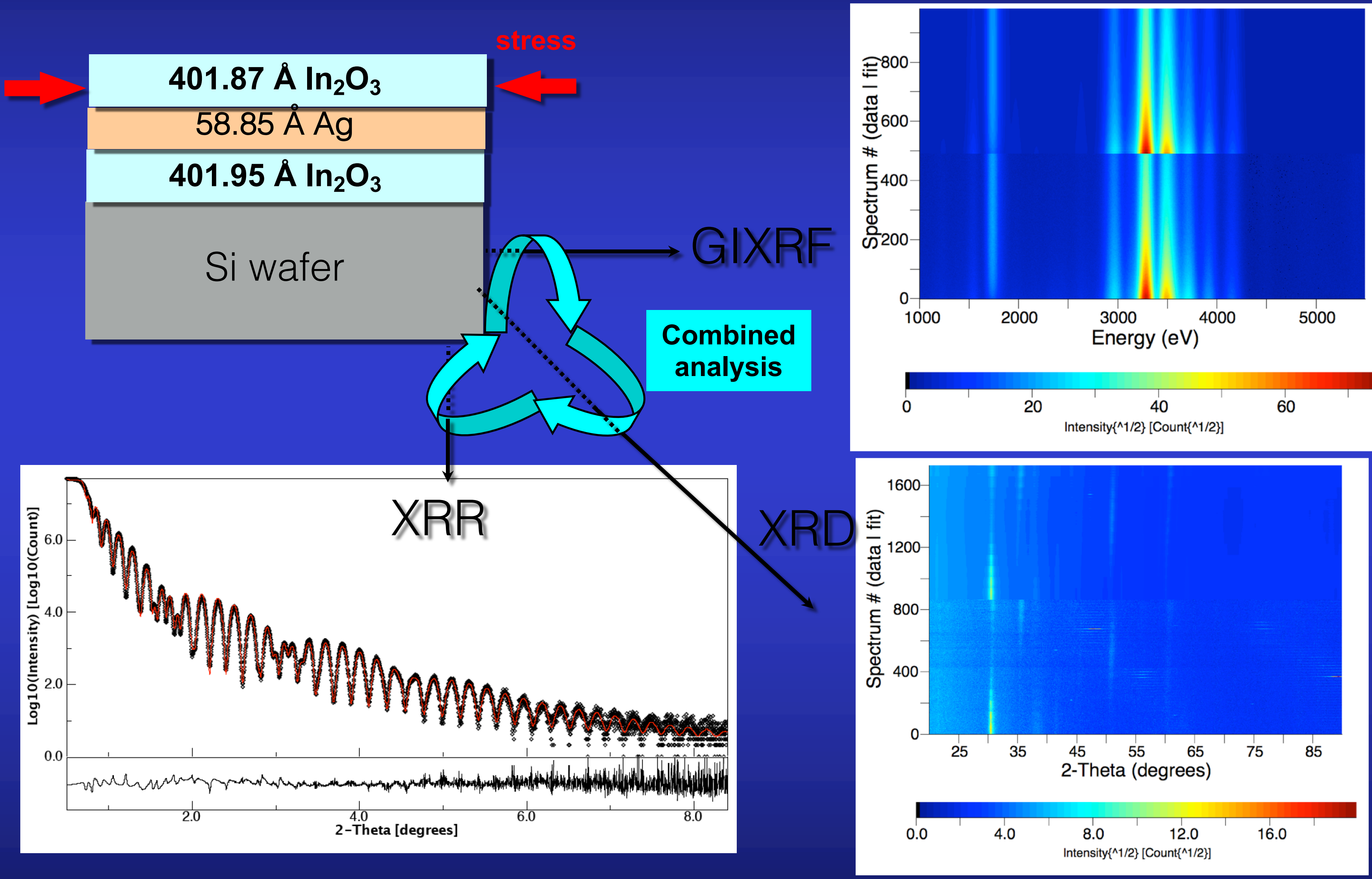

XRR

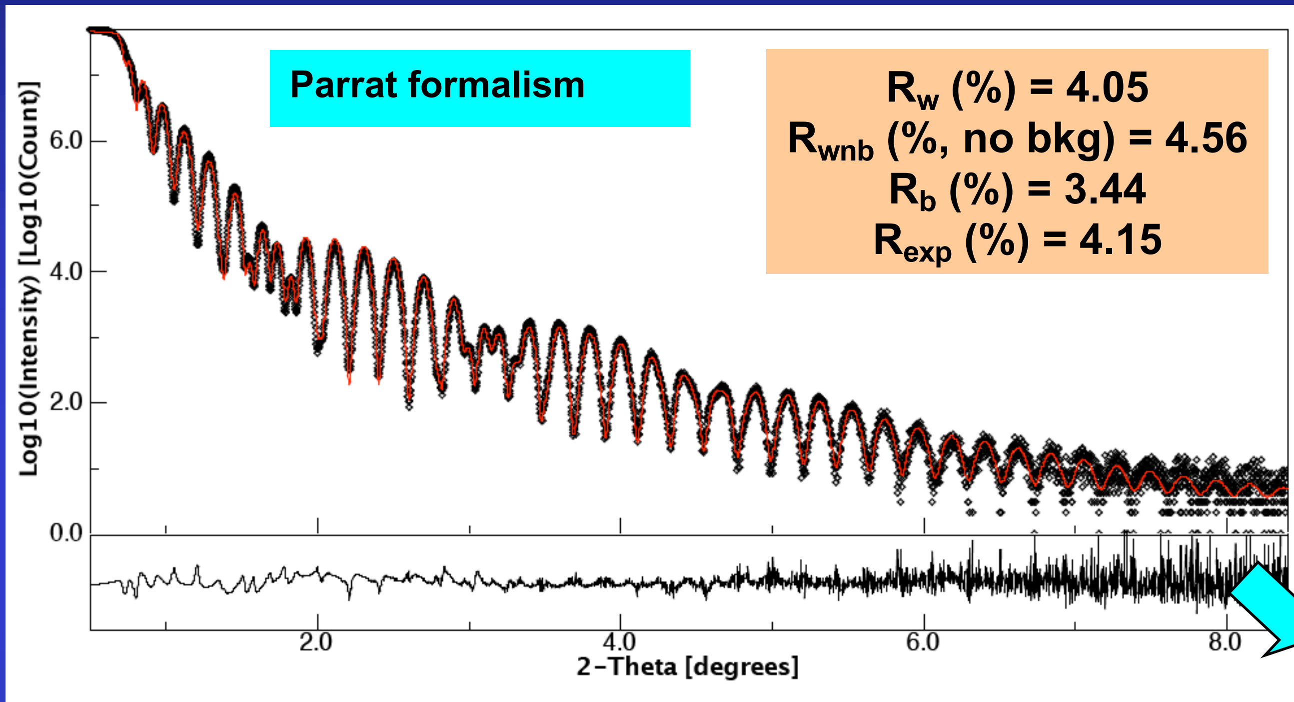

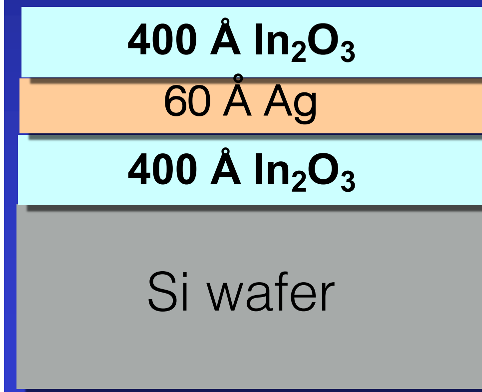

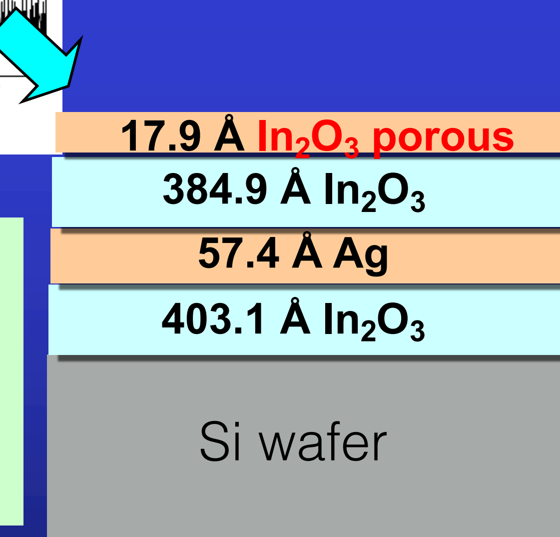

Highly porous In_2O_3 layer

Top layer: q_c = 0.0294 Å^{-1}; roughness r =0.38nm

Top In_2O_3: q_c = 0.0504 Å^{-1}; r =2.06 nm

Ag : q_c = 0.0576 Å^{-1}; r =0.26 nm

Bottom In_2O_3: q_c = 0.04889 Å^{-1}; r =6.74 nm

Si wafer: q_c = 0.0313 Å^{-1}; r = 0.73 nm

Caby et al. *Spec. Acta B* **113** (2015) 132

XRD

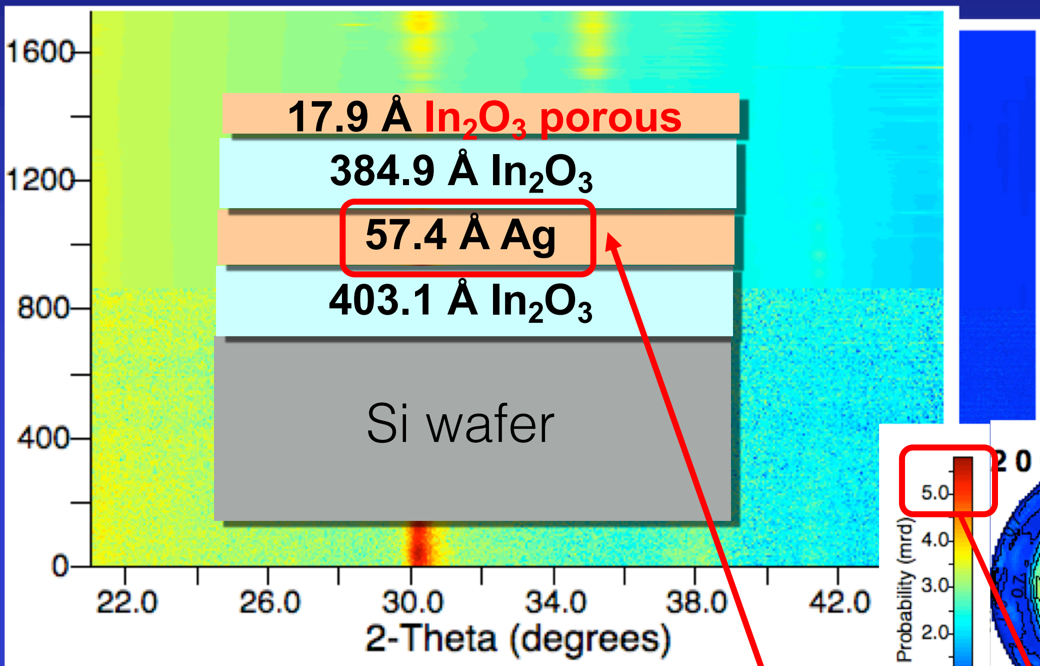

Refined Ag phase parameters

- Isotropic crystallite size = 56.4 (1.3) Å
- Cell parameter: a = 4.0943(7) Å

R_w (%) = 23.97
R_{wnb} (%, no bkg) = 58.31
R_b (%) = 18.71
R_{exp} (%) = 22.04

In_2O_3

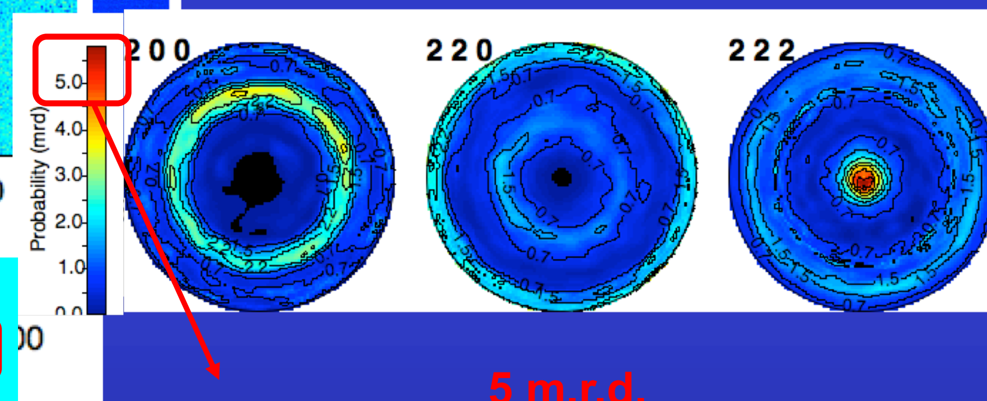

5 m.r.d.

Ag:

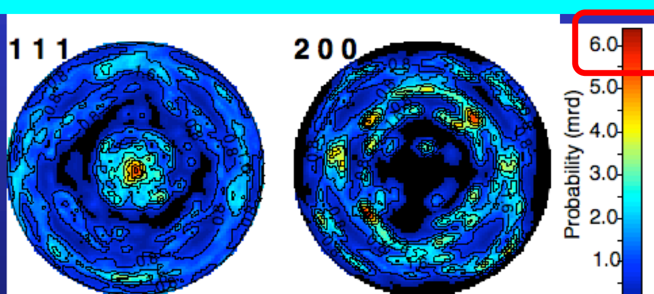

Refined In_2O_3 phase parameters

- σ_{XX} = - 1 GPa (in-plane compressive stress)
- Isotropic crystallite size = 153.2(5) Å
- Cell parameter: a = 10.2104(5) Å

GiXRF

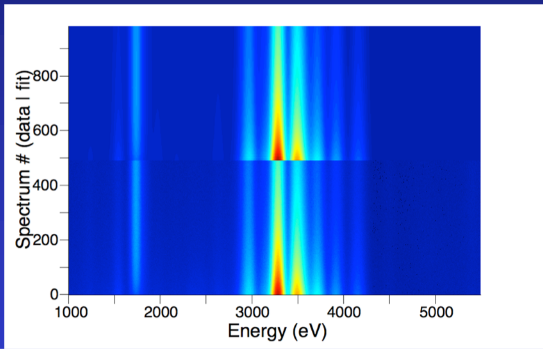

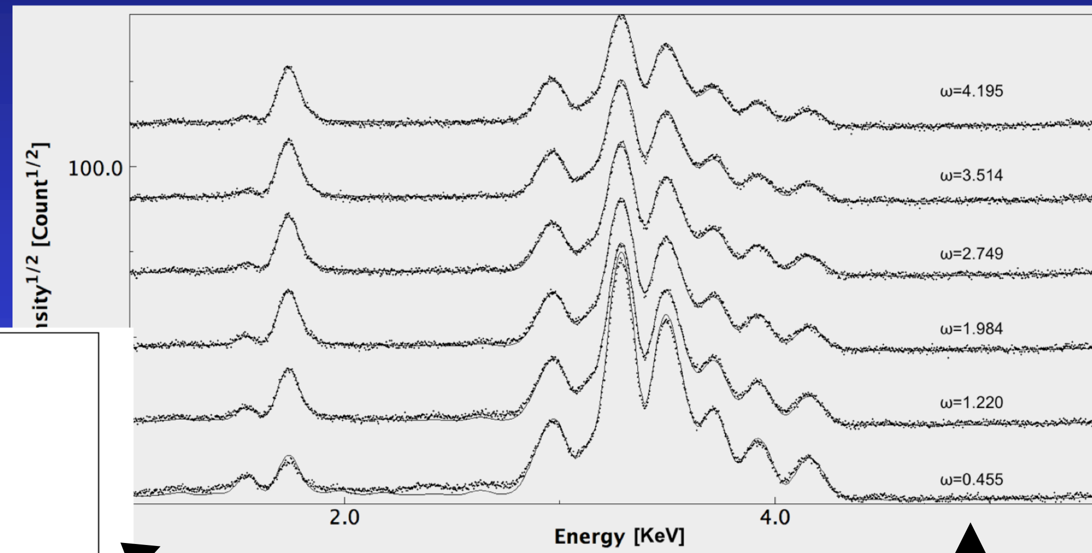

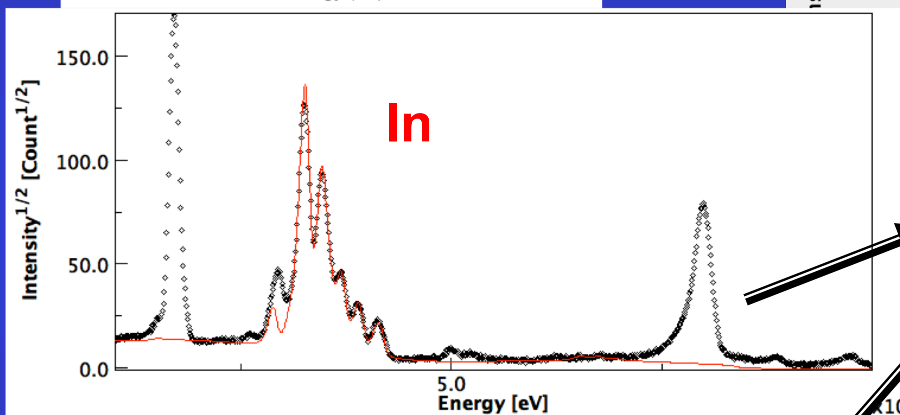

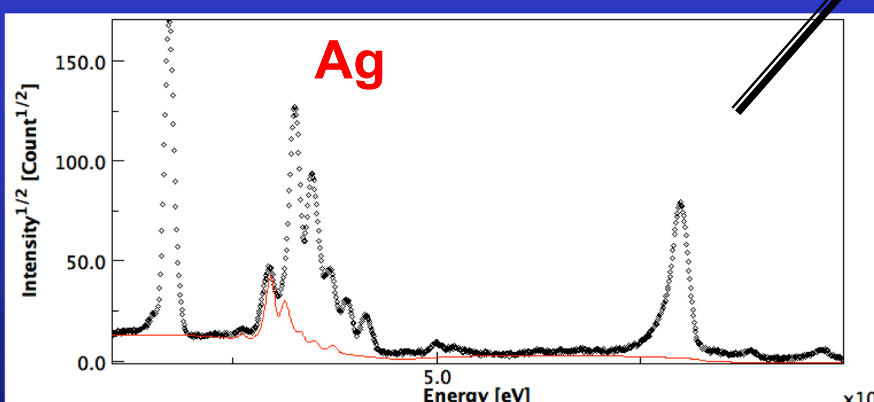

No presence of contaminant observed

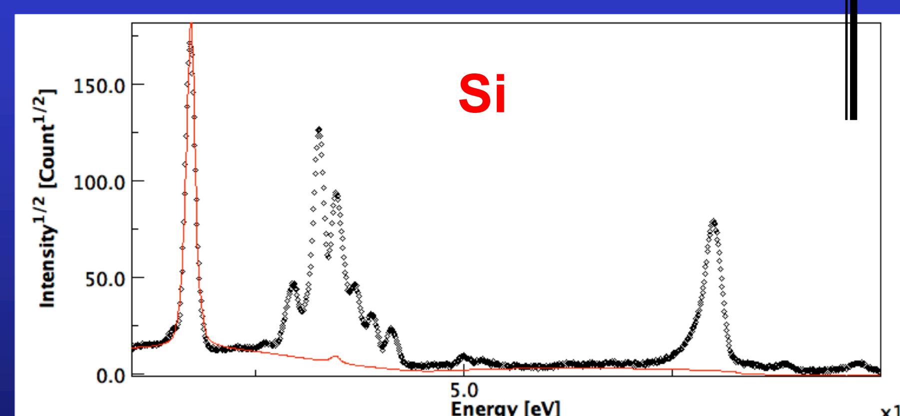

Combined Measurement-Analysis XRD-XRF-Raman for SOLSA

Sequential Acquisition (on-mine real-time)

Hyperspectral 3D imaging

XRD

XRF

Raman

IR

Sonic drilling

ID2A and B

Conveyor

Global XRD-XRF-Raman-IR
Full-Profile Search-Match
QPA – chemical analysis

Open Databases:
COD
TCOD
ROD …

Combined Analysis

or Combined Measurements and Analysis: → ID1

First Combined XRD-XRF-Raman Measurement
(CRISMAT-CNRS Feb. 2018)

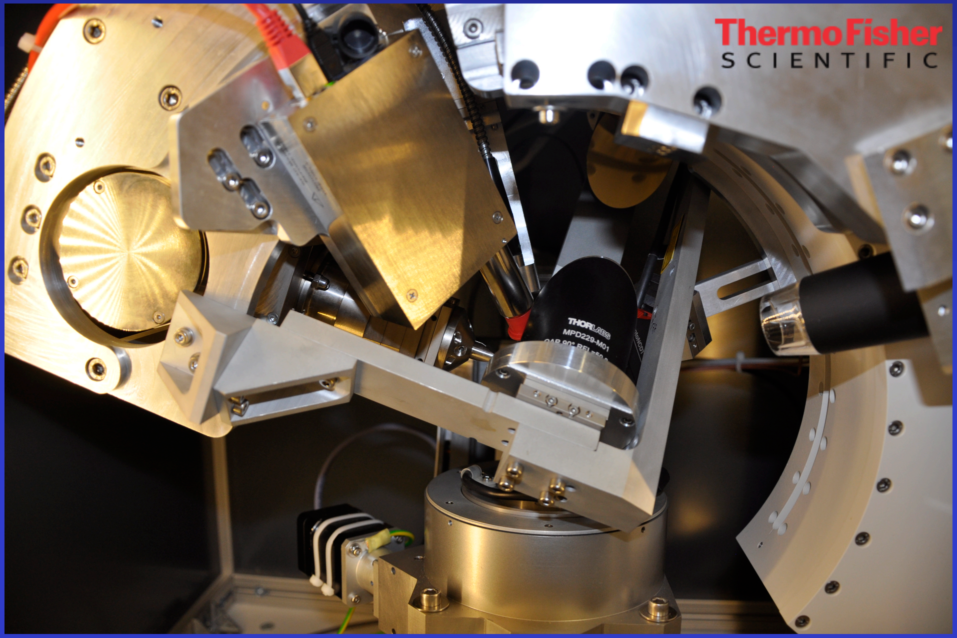

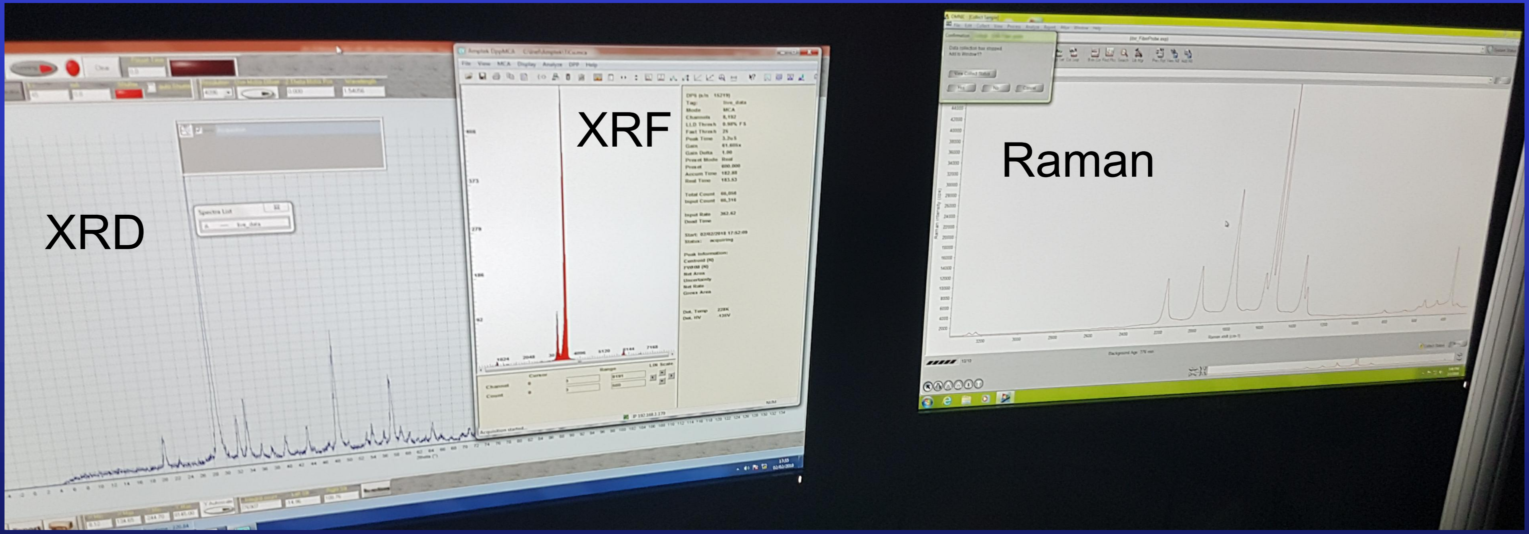

Case study 1: siliceous breccia

a rock originated form hydrofracturing of ultramafic rocks, mainly composed by quartz

XRF

Element	Wt.%	At.%
Si	43.9	32.3
O	51.8	66.5
Fe	3.1	0.9
Ni	0.7	0.2
Cr	0.2	0.06
Mn	0.05	0.01
Co	0.02	0.005

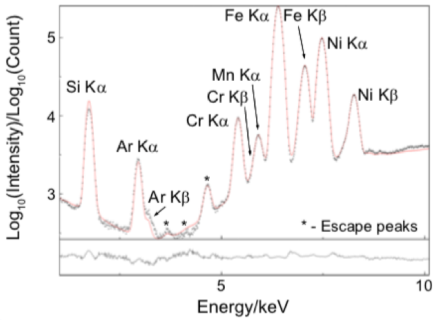

XRD

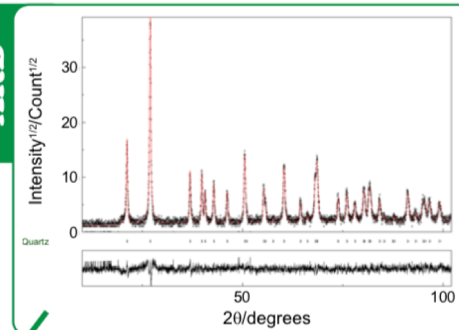

XRD pattern represents solely quartz phase (α-SiO_2)

Fe! **no Fe!**

RS: iron detected by XRF due to iron oxide inclusions, confirmed by SEM and EDXS.

+

XRD: Fe concentration probably below the detection limit (~3 wt.%).

+

XRF gives thus an upper limit of the goethite presence (~5 wt.%), assuming that all the iron (3.1 wt.%) is related to this phase.

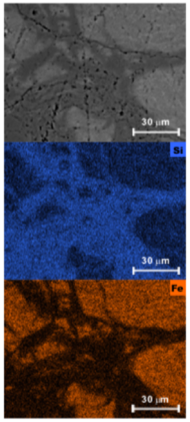

RS

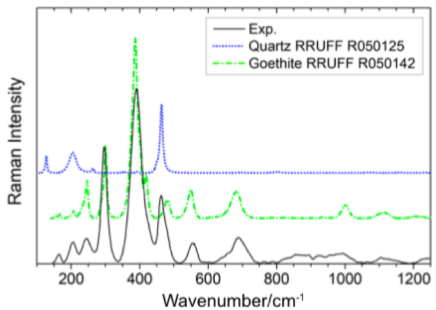

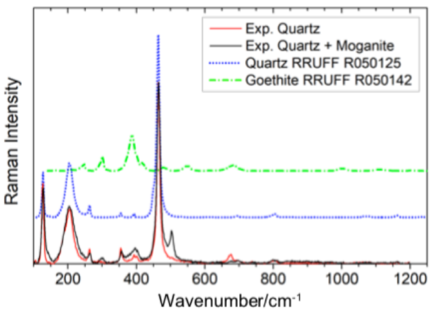

- Dominant phase:
  - quartz (α-SiO_2).
- Minor contribution:
  - moganite (quartz polymorph)
  - goethite (FeO(OH))
  - hematite (α-Fe_2O_3).

WARNING

use of Raman databases: different resolutions vs automatic software

Case study 2: serpentinized harsburgite

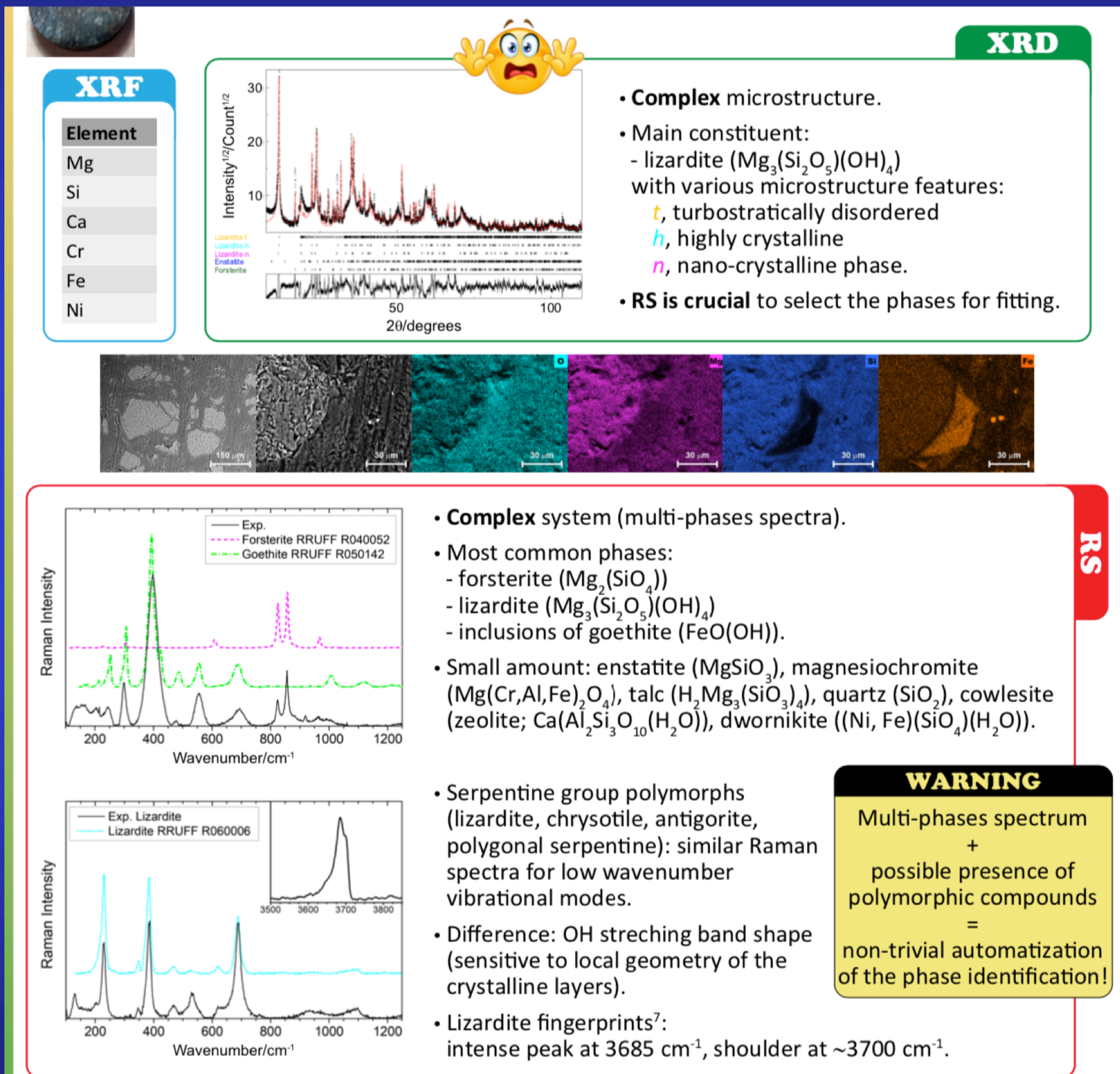

Coarse – medium grains
Composed of orthopyroxene, olivine, serpentine

Lizardite: 76.5 %
Forsterite: 15.8 %
Enstatite: 7.7%

El Mendili et al. *Earth & Space Chem.* (2019)

Case study 3: Dunite

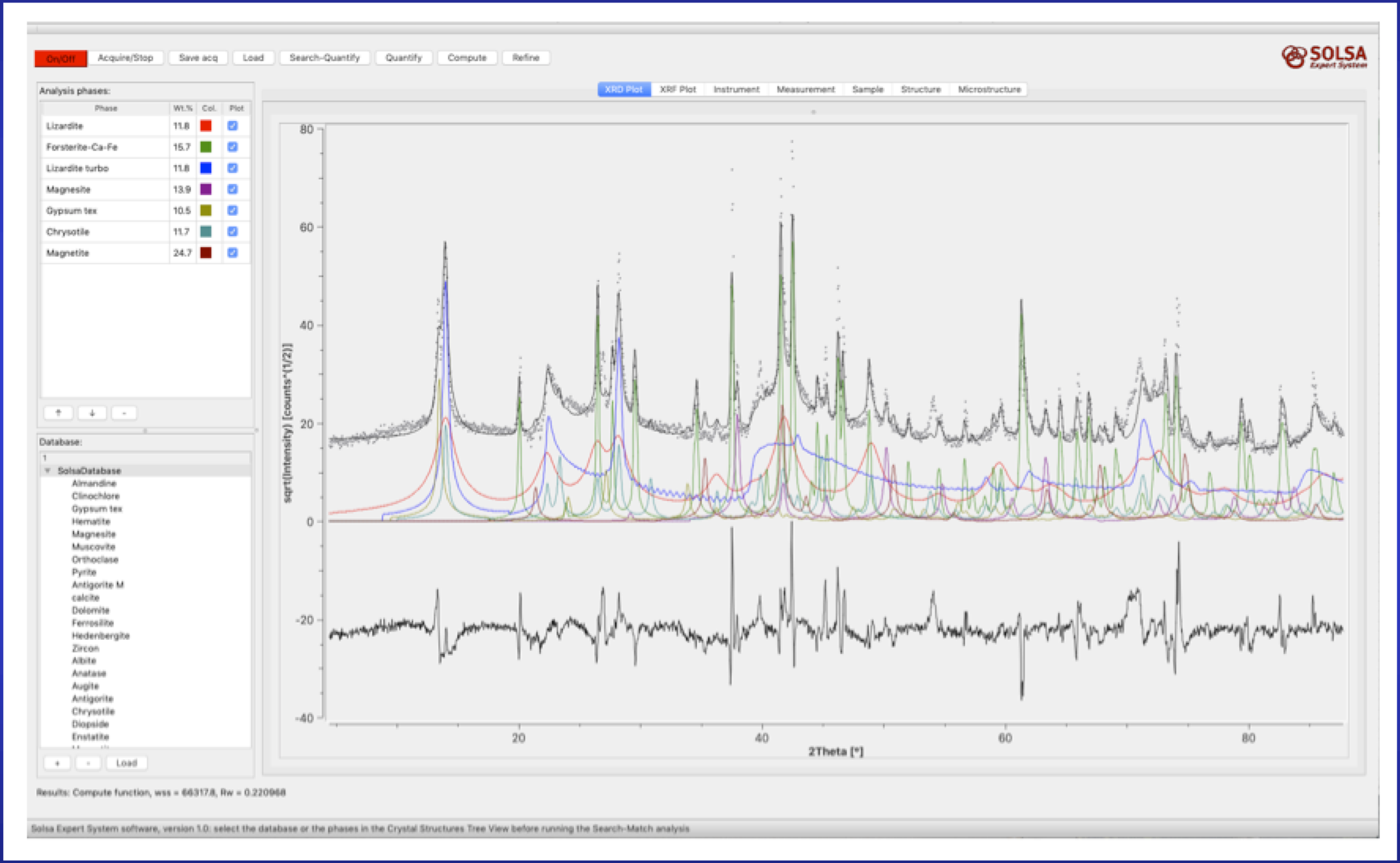

More ?

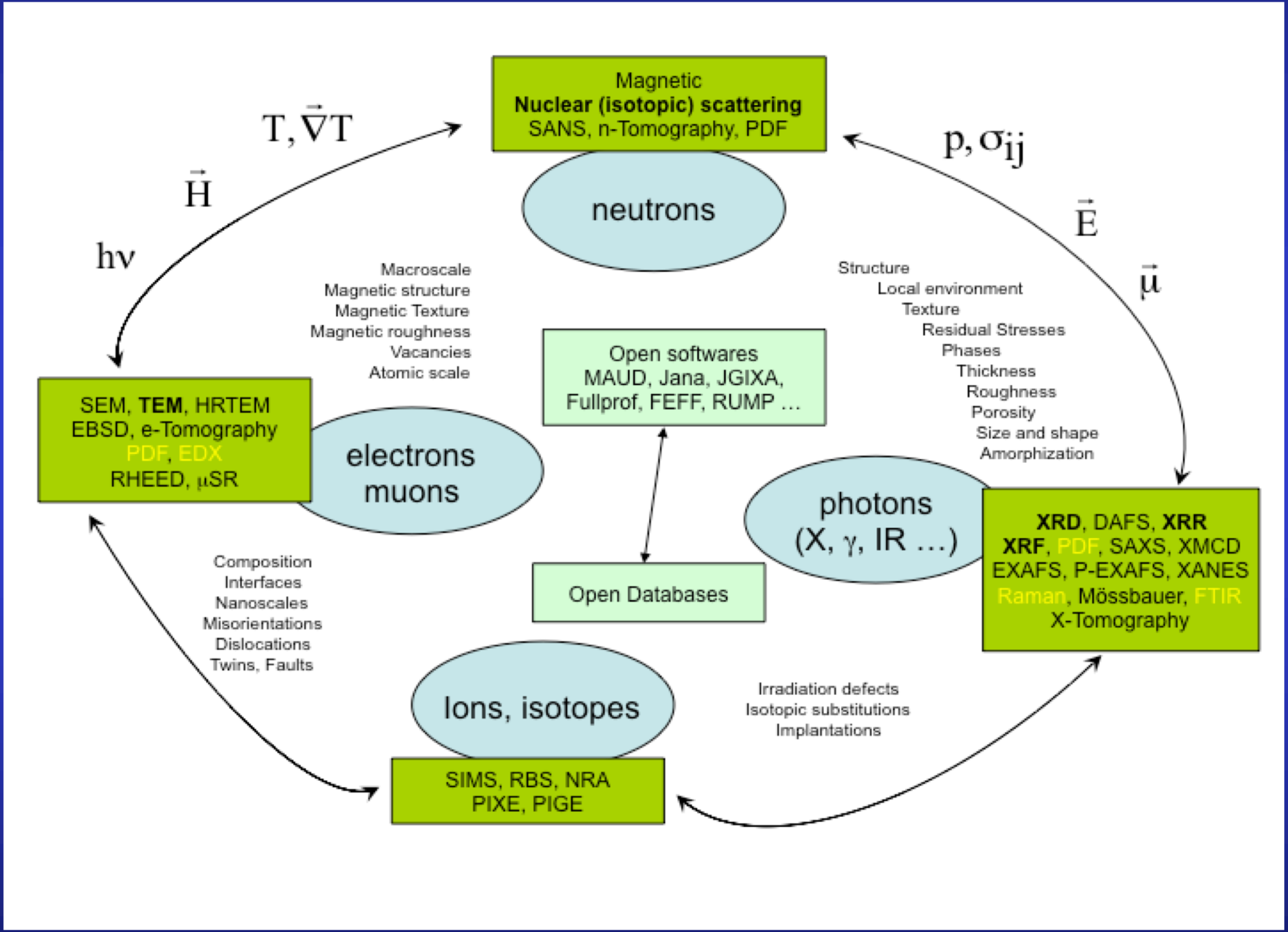

Magnetic
Nuclear (isotopic) scattering
SANS, n-Tomography, PDF
neutrons
$T, \vec{\nabla}T$
$\vec{H}$
$h\nu$
p, σ_{ij}
$\vec{E}$
$\vec{\mu}$
Macroscale
Magnetic structure
Magnetic Texture
Magnetic roughness
Vacancies
Atomic scale
Structure
Local environment
Texture
Residual Stresses
Phases
Thickness
Roughness
Porosity
Size and shape
Amorphization
Open softwares
MAUD, Jana, JGIXA,
Fullprof, FEFF, RUMP …
SEM, TEM, HRTEM
EBSD, e-Tomography
PDF, EDX
RHEED, μSR
electrons
muons
photons
(X, γ, IR …)
XRD, DAFS, XRR
XRF, PDF, SAXS, XMCD
EXAFS, P-EXAFS, XANES
Raman, Mössbauer, FTIR
X-Tomography
Open Databases
Composition
Interfaces
Nanoscales
Misorientations
Dislocations
Twins, Faults
Ions, isotopes
Irradiation defects
Isotopic substitutions
Implantations
SIMS, RBS, NRA
PIXE, PIGE

Combined Analysis Workshop series:
Next one in Caen 24th - 28th June 2024

chateigner.ensicaen.fr/formation/

Thanks !

UNION EUROPENNE

ESQUI
SOLSA

MEET
MIND
Xmat
COSTs

l'Europe s'engage en Basse-Normandie avec le FEDER

COMBIX: Chair of Excellence

AGENCE NATIONALE DE LA RECHERCHE ANR

FURNACE
ECOCORAIL

DAME
SEMOME

Région Centre

SMAM